# REPORT

## MATERIALS SCIENCE

# Impact-resistant nacre-like transparent materials

Z. Yin, F. Hannard, F. Barthelat*

Glass has outstanding optical properties, hardness, and durability, but its applications are limited by its inherent brittleness and poor impact resistance. Lamination and tempering can improve impact response but do not suppress brittleness. We propose a bioinspired laminated glass that duplicates the three-dimensional "brick-and-mortar" arrangement of nacre from mollusk shells, with periodic three-dimensional architectures and interlayers made of a transparent thermoplastic elastomer. This material reproduces the "tablet sliding mechanism," which is key to the toughness of natural nacre but has been largely absent in synthetic nacres. Tablet sliding generates nonlinear deformations over large volumes and significantly improves toughness. This nacre-like glass is also two to three times more impact resistant than laminated glass and tempered glass while maintaining high strength and stiffness.

Glass is a widely used material because of its optical properties, hardness, durability, and thermal and chemical stability. However, glass has no large deformation or toughening mechanism at ambient temperature, and as a result, its tensile strength is compromised by the slightest defects or damage (*1*), and it has poor impact resistance. A strategy to improve strength and impact resistance is tempering, in which compressive stresses are created at the surface of the component to hinder crack initiation, increasing strength to two to five times that of annealed glass (*2*). However, fracturing tempered glass results in catastrophic failures that release the elastic energy stored during tempering, destroying the entire component in an "explosive" fashion. Another strategy consists of intercalating glass sheets with softer polymeric layers to form laminated glass. In case of fracture, the polymeric interlayer holds the glass fragments together, but the overall impact resistance is not otherwise improved significantly (*3*). Tempering and laminating can be used simultaneously, but these methods do not truly increase fracture toughness, and glass components remain by far the weakest structural elements in vehicles, buildings, and electronic devices.

Biological materials can inspire new alleys to overcome brittleness. Now a model for bioinspiration, nacre from mollusk shells is a highly regular three-dimensional brick-and-mortar assembly of microscopic mineral tablets bonded by biopolymers. Under tensile forces, millions of tablets can slide on one another over large volumes (~1 mm$^3$) (*4–6*), a mechanism mediated by the shearing of the interfaces (Fig. 1A). The sliding mechanism dissipates large amounts of mechanical energy, which makes nacre deformable and tough despite its very high mineral content (95 volume %) (*7–9*). Despite three

Department of Mechanical Engineering, McGill University, Montreal, Quebec H3A 2K6, Canada.
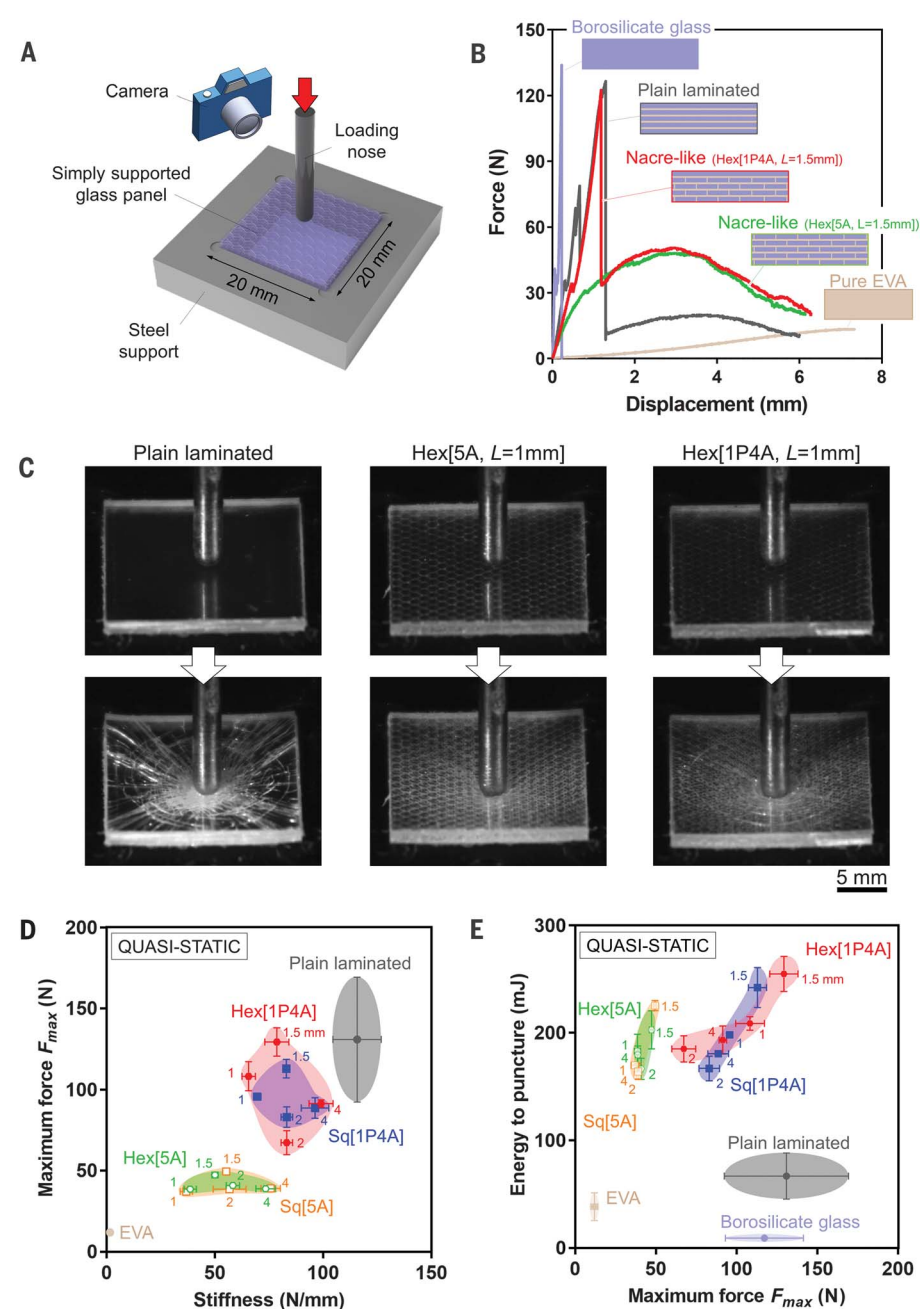*Corresponding author. Email: francois.barthelat@mcgill.ca
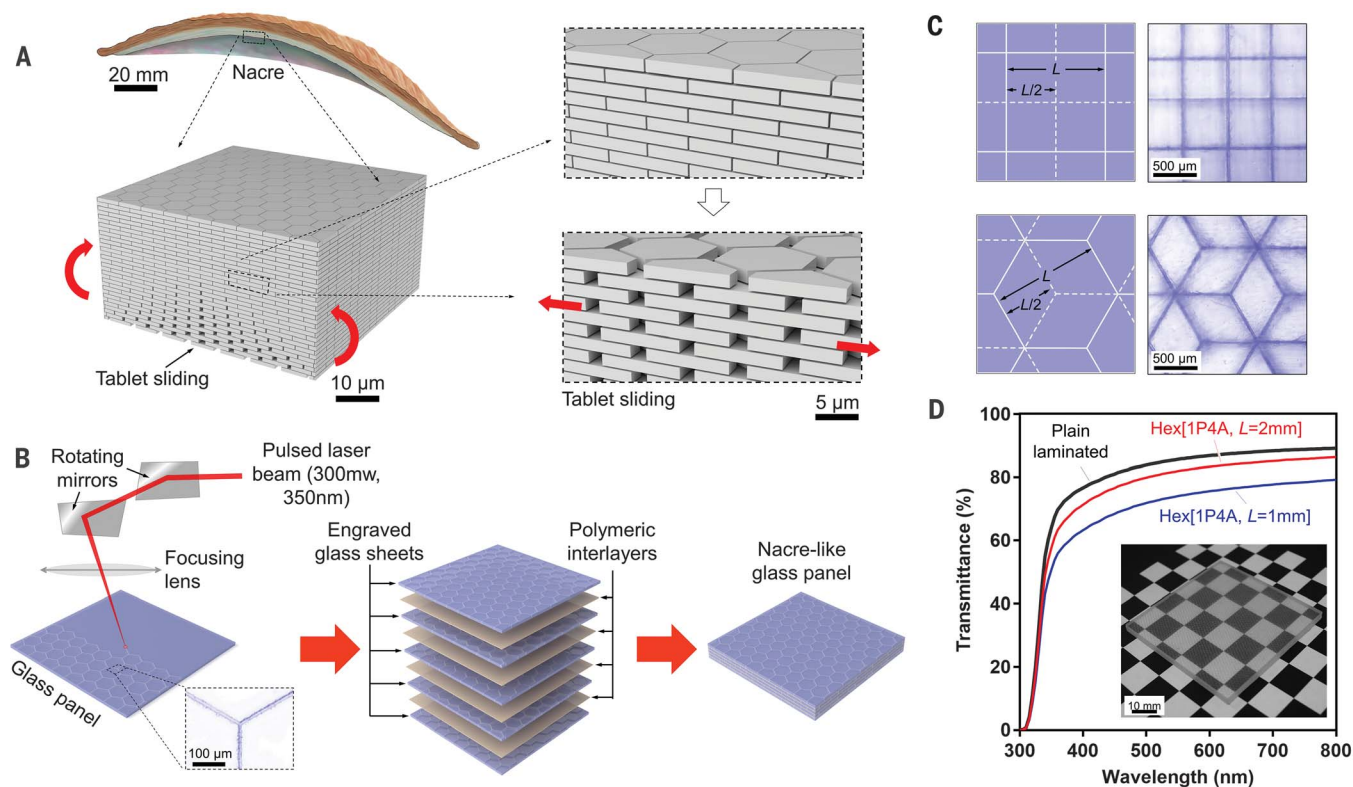


**Fig. 1. Design and fabrication of nacre-like glass panels.** (**A**) Natural nacre is made of 95 volume % of mineral tablets bonded by a softer organic mortar. Nacre can deform, stop cracks, and absorb impact energy by the sliding of the microtablets on one another and over large volumes. (**B**) Fabrication protocol for nacre-like glass panels (scale bar: 100 μm). (**C**) Details of tablet geometry and overlap structure (scale bar: 500 μm). (**D**) Light transmittance of nacre-like glass panels compared with plain laminated panels. (Inset) Optical clarity of a typical engraved panel (scale bar: 10 mm).

decades of research efforts, fabricating large volumes of microscopic nacre-like "brick walls" remains a major challenge (10–15). Fracture toughness is increased significantly in existing nacre-like materials but mainly from crack deflection and crack bridging (14, 16) [mechanisms that are also used in multilayered ceramics (17, 18)]. Ductility can be achieved in nacre-like nanocomposites but at the expense of stiffness and strength (11, 19). Some of these nacre-like materials are transparent, but they only come in the form of thin films (20, 21). Large-scale tablet sliding, which is the critical mechanism in natural nacre (Fig. 1A), has been largely absent in synthetic nacres because the requirements for this mechanism are stringent: (i) hard tablets with a high aspect ratio to transfer shear stresses but not too high to prevent tablet fracture (8, 9), (ii) strong adhesion of the interface material to the mineral (22), (iii) interfaces that are orders of magnitude more compliant than the tablets to achieve a near-uniform shear stress transfer (23), (iv) interface highly deformable in shear to maximize deformability (7), (v) strain hardening at the interface to delay strain localization and maximize the spreading of nonlinear deformations (5), and (vi) size and arrangement of the tablets as uniform as possible to delay strain localization and maximize energy dissipation (24). The synthetic nacres that could fulfill these requirements were fabricated at millimeter scales, allowing high control over material architecture (25–27). These materials achieved extensive tablet sliding but only in one plane, along one direction, and under simple, uniaxial loading.

We report a three-dimensional synthetic nacre-like material that embodies the requirements for tablet sliding and overcomes the inherent brittleness of glass. The contours of the tablets were first engraved on 220-μm-thick borosilicate glass sheets by using a focused pulsed laser beam (28) (Fig. 1B). The engraved lines were sufficiently strong to enable the handling of individual glass sheets without separating the tablets yet weak enough so that individual tablets were separated in a controlled fashion at later stages in the lamination process (28). Five engraved glass sheets were laminated with ~125-μm-thick polymeric interlayers. During assembly, the glass sheets were carefully aligned so that the tablets formed a three-dimensional staggered arrangement akin to natural nacre (Fig. 1B). We fabricated nacre-like panels based on square tablets and based on hexagonal tablets (Fig. 1C) of different sizes [length ($L$) = 1 mm, 1.5 mm, 2 mm, and 4 mm]. These dimensions were chosen to create tablets with an aspect ratio in the order of 10, which is close to the mineral tablets in natural nacre. A critical step was to identify synthetic polymers with mechanical attributes similar to the interfaces in nacre (22). Most of the transparent polymers we tested in shear were too brittle (resulting in poor energy absorption) and/or too strong (resulting in unwanted fracture of the glass tablets) (28). Ethylene-vinyl acetate (EVA) was eventually selected as the interface
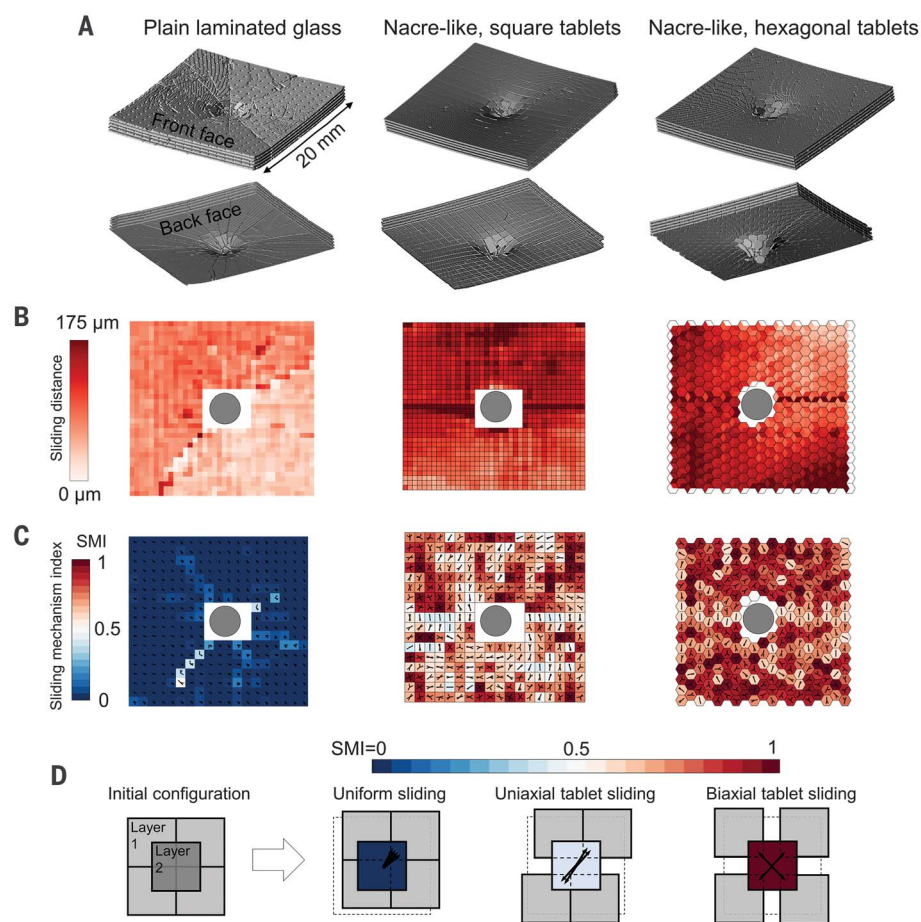
material because of its relatively low strength, very high deformability in shear (>800%), strain hardening, and high energy absorption. EVA is also more resistant to ultraviolet light than polyvinyl butyral (29), another transparent polymer that is used in standard laminated glass. Nacre-

like EVA-glass beams were deformed by large-scale sliding of the tablets (fig. S4), with an estimated work of fracture of 7200 J/m² (28) [more than three times higher than the work of fracture of synthetic nacres made by freeze casting (13, 14)].



**Fig. 2. Puncture of small nacre-like glass panels.** (**A**) Experimental setup: A simply supported glass panel is punctured with a loading nose at a quasi-static rate. (**B**) Puncture force–displacement curves for pure borosilicate glass and pure EVA panels, plain laminated panels, and nacre-like panels with [5A] and [1P4A] layer configurations. (**C**) Plain laminated and nacre-like panels before and during puncture (at a displacement = 3 mm). The lighting and background were chosen to highlight the engraving patterns. Scale bar: 5 mm. (**D** and **E**) Property maps showing (D) maximum force (strength) versus stiffness and (E) energy to puncture versus maximum force for different materials and designs.

**Fig. 3. Micro-CT scans and analysis for plain laminated and nacre-like panels.** (**A**) Three-dimensional microtomography perspectives of punctured samples (for plain laminated glass, arrays of microdots were engraved on the surface of the layers to track their relative sliding). (**B**) Maps of the sliding distance in the lowermost interlayer, showing larger and more distributed sliding in the nacre-like designs. (**C**) Maps of the SMI in the lowermost interlayer in the panel, also showing sliding vectors. (**D**) Schematic showing three sliding mechanisms corresponding to three values of the SMI. Tablet sliding was generally more bidirectional and isotropic in panels based on hexagonal tablets.
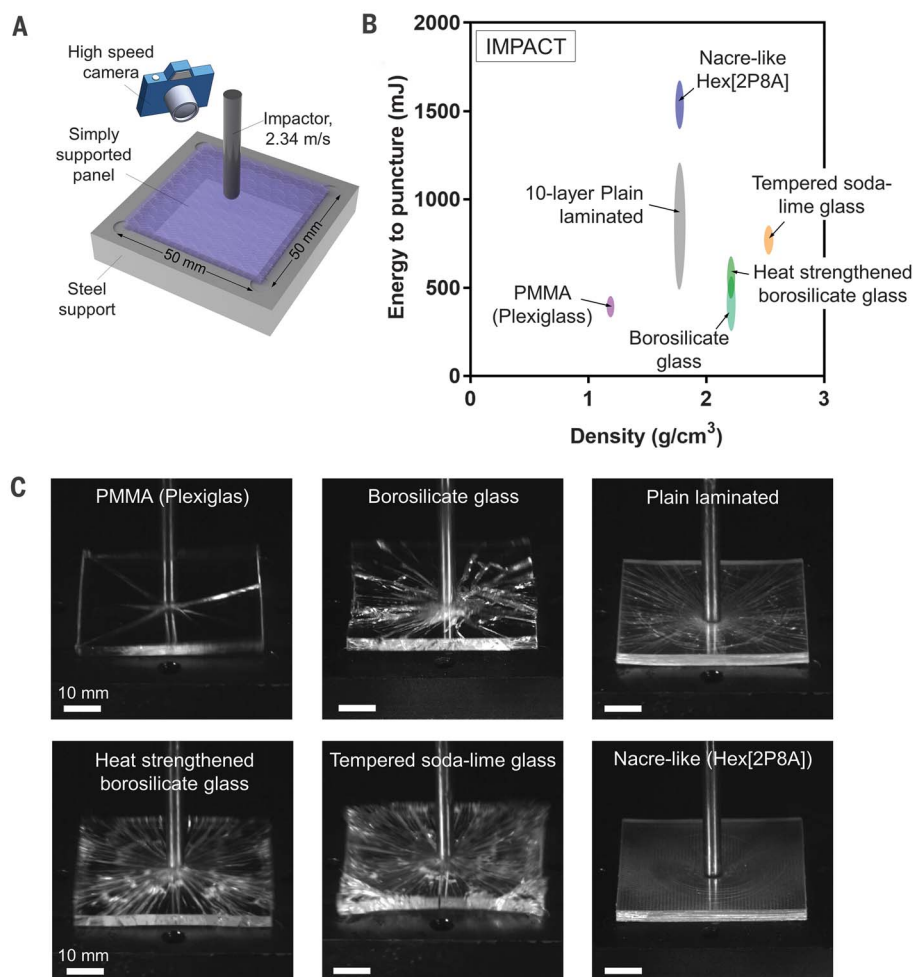
Visually, nacre-like panels are transparent materials that generated relatively little blurring, little haze, and no image distortion (Fig. 1D). Light transmittance in the visible light range was about 10% lower than the transmittance of regular laminated glasses (Fig. 1D). Puncture tests on simply supported (20 mm by 20 mm by 1.6 mm) panels of different designs (Fig. 2A) showed that borosilicate glass and plain laminated glass have a high strength but fail in a brittle fashion (Fig. 2B), with multiple catastrophic cracks emanating from the loading point to the edge of the panel (Fig. 2C). The strength of these materials showed large variability because it is governed by weakest-link (Weibull) statistics (30). In the laminated glass panels, the fragments were held by the EVA interlayers, which produced a small but non-negligible residual puncture force. This mechanism, typical of traditional laminated windows and windshields, only involves a small volume fraction of the EVA interlayer, and therefore the deformation and energy-absorbing capabilities of the interfaces were largely underused. By contrast, the nacre-like panels produced a more ductile response with large deformations and high energy to puncture (area under the force-displacement curve). The mechanical response of the nacre-like glass was more repeatable than in plain and laminated glasses because it is governed by tablet sliding, a well-controlled deterministic mechanism. Damage was overall much less visible compared with regular laminated glass, but a large homogenous and plastic deformation developed around the puncture site (Fig. 2C). Because of their segmented architecture, the stiffness and the strength of the initial all-engraved designs [5A] were about half of the stiffness and strength of laminated glass (Fig. 2D). An improved design with a plain glass sheet used as front layer [designs (1P4A): Fig. 2B] increased the initial strength and stiffness to levels only 10 to 15% below plain laminated glass (Fig. 2D). [Similarly, the strength and stiffness of natural nacre are lower than that of the individual aragonite tablets (22), and the nacreous layer is covered by a harder and stiffer layer of prismatic calcite (31).] The homogenous front glass layer also provides high surface hardness, durability, dimensional stability, and waterproofness. In terms of energy to puncture, plain borosilicate glass performed the worst (Fig. 2E). Laminated glass had an improved (sixfold) energy to puncture, but the nacre-like designs were the toughest, "amplifying" the energy to puncture by another factor of 2.5 to 4 compared with laminated glass. Short tablets ($L = 1$ mm) ensured tablet sliding without tablet failure. By contrast, longer tablets ($L = 2$ mm and $L = 4$ mm) led to higher stiffness, but excessive fracture of individual tablets limited strength and energy absorption. The best nacre-like panel design in terms of high energy to puncture and high strength was the [1P4A] layer configuration with $L = 1.5$-mm hexagonal tablets (Fig. 2E).

Micro–computed tomography (micro-CT) of the punctured panels (28) provided a comprehensive picture of the micromechanics of deformation in laminated glass and in the nacre-like panels (Fig. 3). We were particularly interested in quantifying the amount and type of shear deformation ("sliding") at the interfaces between the glass layers, because it is the main mechanism for energy dissipation (28). The sliding distribution in the lowermost interlayer in the panel (Fig. 3B) shows relatively small interfacial sliding distances in the plain laminated glass, except near large cracks. By contrast, the sliding distances in the nacre-like panels were much larger and more homogenously distributed. On the basis of the sliding distance distributions, we computed the square of the sliding distance integrated over the entire interface, a quantity that scales with energy absorption. The integrated values for the nacre-like panel were about 2.4 times greater than those of the plain laminated glass, in agreement with the puncture tests in which the energy to puncture in the nacre-like panels was 2 to 3 times larger than that of the plain laminated glass. The shear deformation of the interfaces is therefore the main source of toughness in the nacre-like panels. We also computed a sliding mechanism index (SMI) (28), a normalized version of the local divergent of the sliding displacements vector field (Fig. 3D). In plain laminated glass, sliding was mostly uniform (SMI ~0), except in localized regions across the cracks, where SMI ~0.5 (uniaxial separation of fragments). By contrast, the deformation in the nacre-like panels was dominated by unidirectional and biaxial sliding ($0.5 <$ SMI $< 1$), providing quantitative evidence that these panels properly duplicated the nacre-like sliding mechanism over large volumes (Fig. 3C).

We finally tested larger panels (50 mm by 50 mm by 3 mm) for impact resistance (28). Poly(methyl methacrylate) (PMMA) (Plexiglas) was the lightest of the materials tested, but it also had the lowest impact resistance (energy to puncture) (Fig. 4B). This transparent polymer is brittle at high loading rates, and the panel fractured into four to five large fragments (Fig. 4C). Pure borosilicate glass is about twice as dense as

**Fig. 4. Impact tests on large nacre-like panels and other transparent materials.** (**A**) Experimental setup: A simply supported (50 mm by 50 mm by 3 mm) panel is impacted at a velocity of 2.34 m/s. (**B**) Energy to puncture versus mass density property map for the six designs and materials tested in impact (all had the same overall dimensions). (**C**) Corresponding snapshots from high-speed photography. Scale bar: 10 mm.

PMMA, with a slightly higher impact resistance but also a brittle fracture. The two types of tempered glasses we tested had an improved impact resistance; failure was catastrophic and explosive, with multiple small fragments. Laminated glass performed better than the tempered glasses in terms of impact resistance, because of the large number of layers used ($N$ = 10) and the high deformability of the EVA interlayers. The damage pattern was, however, the same as in the quasi-static regime, with extensive damage in the form of long radial and circumferential cracks and fragments held together by the EVA interlayer. Finally, nacre-like panels based on hexagonal tablets ($L$ = 1.5 mm) and with a [2P8A] configuration [we used two plain layers on the front face of the 10-layer panel to match the composition of the (1P8A) design] had the highest impact resistance, about double that of the tempered glasses. The nacre-like panels also failed by a graceful mode with large inelastic deformations and no shards (Fig. 4C).

Our transparent glass duplicates the large-scale sliding of individual tablets in three dimensions and over large volumes, even when subjected to a concentrated force. This mechanism is mediated by the shearing of the interlayers, which absorbs large amounts of mechanical energy, providing the material with toughness, superior impact resistance, graceful failure, and damage tolerance. These nacre-like panels also illustrate how an architecture with relatively large size but with high order and periodicity can be preferable to smaller but more disordered microstructures, which is consistent with recent models and other recent bioinspired materials (*24, 32*). Finally the laser engraving and lamination fabrication methods are inexpensive and relatively easy to implement into the large-scale production of impact-resistant nacre-like glass panels for a wide range of applications, including protective structures, windows, photovoltaic systems, building materials, and electronic devices.

## REFERENCES AND NOTES

1. Z. W. Zhong, Y. B. Tian, T. G. Xie, *Int. J. Adv. Manuf. Technol.* **87**, 3261–3269 (2016).
2. H. Carré, L. Daudeville, *J. Eng. Mech.* **125**, 914–921 (1999).
3. H. S. Norville, K. W. King, J. L. Swofford, *J. Eng. Mech.* **124**, 46–53 (1998).
4. R. Z. Wang, Z. Suo, A. G. Evans, N. Yao, I. A. Aksay, *J. Mater. Res.* **16**, 2485–2493 (2001).
5. F. Barthelat, H. Tang, P. Zavattieri, C. Li, H. Espinosa, *J. Mech. Phys. Solids* **55**, 306–337 (2007).
6. A. P. Jackson, J. F. V. Vincent, R. M. Turner, R. M. Alexander, *Proc. R. Soc. London Ser. B* **234**, 415–440 (1988).
7. F. Barthelat, R. Rabiei, *J. Mech. Phys. Solids* **59**, 829–840 (2011).
8. M. R. Begley *et al.*, *J. Mech. Phys. Solids* **60**, 1545–1560 (2012).
9. F. Barthelat, *J. Mech. Phys. Solids* **73**, 22–37 (2014).
10. S. Behr, U. Vainio, M. Müller, A. Schreyer, G. A. Schneider, *Sci. Rep.* **5**, 9984 (2015).
11. P. Das *et al.*, *Nat. Commun.* **6**, 5967 (2015).
12. L. J. Bonderer, A. R. Studart, L. J. Gauckler, *Science* **319**, 1069–1073 (2008).
13. E. Munch *et al.*, *Science* **322**, 1516–1520 (2008).
14. F. Bouville *et al.*, *Nat. Mater.* **13**, 508–514 (2014).
15. R. M. Erb, R. Libanori, N. Rothfuchs, A. R. Studart, *Science* **335**, 199–204 (2012).
16. M. Morits *et al.*, *Adv. Funct. Mater.* **27**, 1605378 (2017).
17. W. J. Clegg, K. Kendall, N. M. Alford, T. W. Button, J. D. Birchall, *Nature* **347**, 455–457 (1990).
18. K. Livanov *et al.*, *J. Am. Ceram. Soc.* **98**, 1285–1291 (2015).
19. B. Zhu *et al.*, *Angew. Chem. Int. Ed. Engl.* **54**, 8653–8657 (2015).
20. T. Ebina, F. Mizukami, *Adv. Mater.* **19**, 2450–2453 (2007).
21. Y. Liu, S.-H. Yu, L. Bergström, *Adv. Funct. Mater.* **28**, 1703277 (2018).
22. F. Barthelat, Z. Yin, M. J. Buehler, *Nat. Rev. Mater.* **1**, 16007 (2016).
23. F. Barthelat, A. K. Dastjerdi, R. Rabiei, *J. R. Soc. Interface* **10**, 20120849 (2012).
24. N. Abid, M. Mirkhalaf, F. Barthelat, *J. Mech. Phys. Solids* **112**, 385–402 (2018).
25. H. D. Espinosa *et al.*, *Nat. Commun.* **2**, 173 (2011).
26. S. M. Valashani, F. Barthelat, *Bioinspir. Biomim.* **10**, 026005 (2015).
27. L. S. Dimas, G. H. Bratzel, I. Eylon, M. J. Buehler, *Adv. Funct. Mater.* **23**, 4629–4638 (2013).
28. Materials and methods are available as supplementary materials.
29. T. Serafinavičius, J.-P. Lebet, C. Louter, T. Lenkimas, A. Kuranovas, *Procedia Eng.* **57**, 996–1004 (2013).
30. B. Lawn, *Fracture of Brittle Solids* (Cambridge Univ. Press, 1993).
31. J. D. Taylor, M. Layman, *Palaeontology* **15**, 73–87 (1972).
32. Z. Yin, A. Dastjerdi, F. Barthelat, *Acta Biomater.* **75**, 439–450 (2018).

## SUPPLEMENTARY MATERIALS

science.sciencemag.org/content/364/6447/1260/suppl/DC1
Materials and Methods
Supplementary Text
Figs. S1 to S6
Movies S1 to S3
References (*33–40*)